Journal of
Nuclear Engineering

MDPI

Article

Optimization Strategies to Improve the Safety Behaviour of a Soluble-Boron-Free SMR Core During a Rod Ejection Accident

Yi Song * and Victor Hugo Sanchez-Espinoza

Mechanical Engineering Faculty, Karlsruhe Institute of Technology (KIT), Hermann-vom-Helmholtz-Platz-1, 76344 Eggenstein-Leopoldshafen, Germany; victor.sanchez@kit.edu
* Correspondence: songyibao0311@gmail.com

Abstract

Soluble-boron-free designs for water-cooled small modular reactors offer advantages such as reduced corrosion and simplified systems. However, the absence of soluble boron necessitates higher total control rod worth for reactivity control and the shutdown margin, leading to excessive individual control rod worth, which can lead to severe power excursions during a rod ejection accident (REA), potentially threatening the fuel integrity and core-cooling capability. The analysis of a hypothetical REA for an equilibrium core design showed that the fuel rod cladding failed due to the high reactivity worth of the ejected control rod. To enlarge the safety margins of this design under accidental conditions, two strategies were adopted: implementing a hybrid control rod configuration to decrease the local reactivity worth within single fuel assembly and re-arranging the refuelling loading pattern to prevent fresh fuel clustering. Using an in-house CoreOptimizer tool, the CASMO5 and SIMULATE5 simulations were automatized to find out an optimized equilibrium core design. The results demonstrated that all safety parameters of the optimized equilibrium core designs are within regulatory limits during normal operation and under REA conditions. By reducing the individual control rod worth, power spikes are considerably mitigated, thereby ensuring fuel integrity during an REA.

Keywords: soluble-boron-free; SMR; equilibrium cycle; rod ejection accident

1. Introduction

Water-cooled (WC) small modular reactors (SMRs) have advantages compared with large pressurized water reactors (PWRs) thanks to their small size and modular fabrication, low initial capital investment, scalability, siting flexibility, etc. These features make WC-SMRs attractive for diverse applications such as electricity generation, district heating, industrial processes, water desalination, and hydrogen production. Different WC-SMR projects include the ACP-100 (China) [1], SMART100 (South Korea) [2] and Rolls-Royce SMR (UK) [3].

Some innovative WC-SMR concepts are based on soluble-boron-free (SBF) core designs, which aim to reduce corrosion and simplify the reactor system. Many SBF SMRs are under development, such as RITM-400 [4], LDR-50 SMR [5], i-SMR [6], PRATIC [7], and KSMR [8].

However, the elimination of soluble boron leads to the SBF SMR cores relying entirely on burnable absorber (BA) and control rods (CRs) for reactivity control, introducing challenges to core design and safety. Since only CRs are movable, core power non-uniformity is highly dependent on the axial position of the control rods. Therefore, the core design must not only reasonably balance fuel enrichment and BA concentration but also optimize the

Academic Editor: Dan Gabriel Cacuci

Received: 11 February 2026
Revised: 3 June 2026
Accepted: 5 June 2026
Published: 23 June 2026

control rod configuration during the multicycle depletion. The configuration of the control rods must satisfy two safety objectives [9]:

- Safety banks must ensure adequate shutdown margins under all operational conditions, including scenarios with a single stuck control rod.
- Core coolability must be maintained during postulated accidents such as a rod ejection accident (REA), in which the regulating bank in one fuel assembly is accidently ejected due to a mechanical failure.

This behaviour is particularly pronounced in SBF SMRs due to the following reasons: Without the soluble boron to control the reactivity, the total control rod worth in a SBF core must be higher than in a boron-based core to ensure shutdown capability over the full cycle length. Moreover, the smaller core size of SMRs leads to greater neutron leakage, often necessitating higher fuel enrichment, further increasing the core's excess reactivity. These factors elevate the total control rod worth and potentially increases the individual CR worth.

Comparative studies highlight these trends. In boron-based SMRs such as SMART and NuScale, REAs with ejected control rod worths of 0.299$ and 0.23$ resulted in peak power levels of 212% and 104% of the nominal power, respectively [10,11]. In contrast, an REA performed in a soluble-boron-free SMR core [12,13] using PARCS coupled with SUBCHANFLOW reported that the normalized reactivity reached 1.4$, driving the total core power to a peak of 5000% of its nominal value. Despite the considerable power excursion, the fuel-cladding integrity and core coolability were concluded to be not threatened.

Following the optimization approach established in [10], this investigation used CASMO5 [14] for cross-section generation and SIMULATE5 [15] for predicting the core behaviour along the core depletion. The CoreOptimizer described in [16] automated the input generation, execution and data extraction for both codes.

In this study, starting from the core design described in [16], two control rod layouts were evaluated under steady-state conditions to identify the configuration with the lowest peak reactivity worth ρ($) for subsequent REA analysis. The primary goal was to demonstrate the optimized core design maintains sufficient safety margins during an REA while satisfying overall steady-state safety criteria and providing sufficient shutdown margin.

This paper is structured as follows: Following this Introduction, Section 2 provides a brief description of behaviour of the initial core design during an REA, showing violation of the safety criteria. To address the issue, Section 3 then introduces the two core optimization strategies and briefly describe the optimization process. Finally, Section 4 presents a comprehensive analysis of the optimized core behaviour, including safety parameters during normal operation, shutdown margin, and transient responses during an REA. Finally, main conclusions and outlook will be described.

2. Behaviour of the Previous Core Design Under REA-Conditions

An equilibrium SBF SMR core configuration was designed [10] using an automated tool CoreOptimizer, integrated with CASMO5 and SIMULATE5. The primary objective was to identify a core configuration demonstrating steady-state safety performance as burnup, while transient behaviour was not initially taken into account. To further improve this core design, an REA was subsequently analyzed. However, the results indicate that fuel cladding integrity would be threatened during an REA. In this section, the previous core design is briefly described, followed by an analysis of REA results for this core. Additionally, the potential factors that may lead to fuel failure during an REA are proposed, providing a basis for the subsequent improvements.

2.1. Brief Description of the Previous Core Design

The core consisted of 57 fuel assemblies arranged in square lattices, with an active core height of 2.0 m. The geometrical data and operating conditions are displayed in [16].

The core radial loading patterns and control rod radial layouts are illustrated in Figure 1. Notably, the fuel assemblies and control rods are axially homogeneous. The variables of the multi-fuel-zones are detailed on Figure 1, including the fuel enrichment (ENR), burnable absorber number per assembly (BA per FA), and the burnable absorber loading (BA loading). The corresponding fuel assembly arrangement with different numbers of the burnable absorber rods are illustrated in Figure 2. The materials of the regulating and safety control rod banks are also included in Figure 1, including stainless steel (SS), silver–indium–cadmium (AIC), and boron carbide (B_4C).

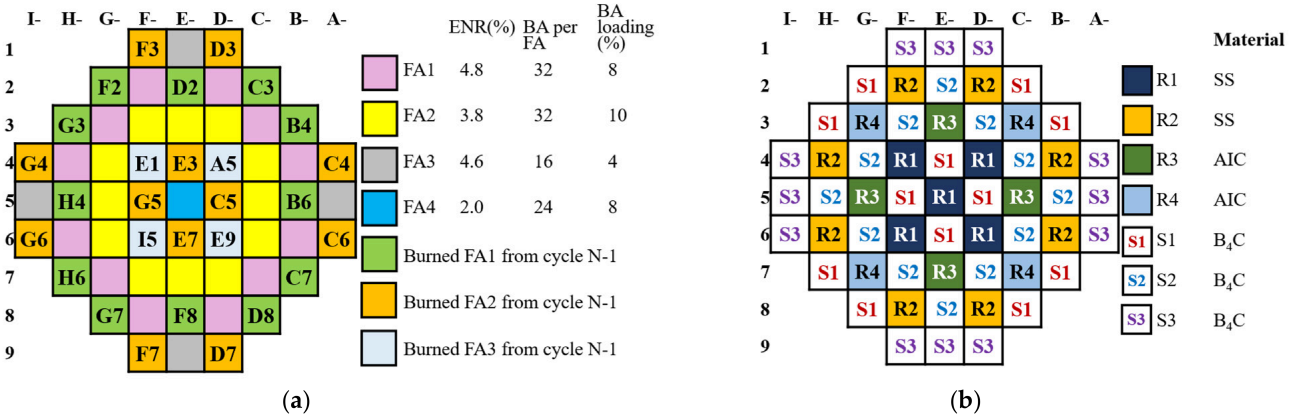

Figure 1. Radial loading pattern (**a**) and control rod radial layouts (**b**) of the previous cores.

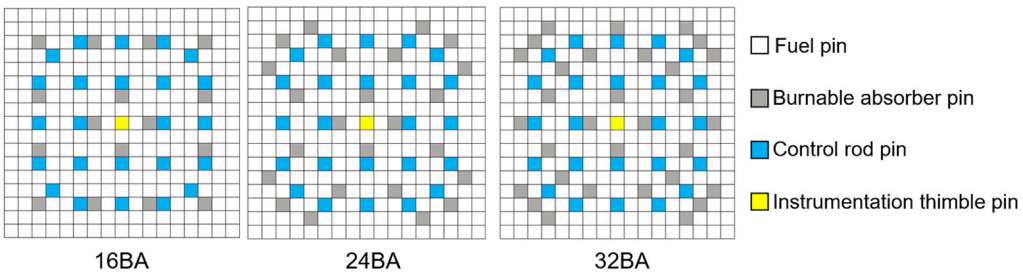

Figure 2. Radial arrangements of the FAs with various BA rods of the previous cores.

2.2. Rod Ejection Accident Analysis in the Previous Core Design

In a previous investigation [16], the safety parameters of the designed equilibrium core during normal operation were analyzed in detail. In the current study, the hypothetical REA simulations were conducted in SIMULATE5-K [17].

2.2.1. Initial Conditions and Assumptions of Rod Ejection Accident Simulations

To evaluate the core's response, the REA simulations incorporated a specific set of initial conditions and assumptions designed to represent challenging scenarios. The initial condition for the REA is hot full power (HFP) with thermal power of 330 MW, a coolant flow rate of 2006.4 kg/s, a coolant inlet temperature of 296 °C and pressure of 15.0 MPa.

For these simulations, the REA was conservatively assumed to be completed within a very short duration of 0.05 s, which is half of the typically assumed REA duration for a standard PWR core [8]. The simulations were run for a duration of 3.0 s to adequately capture the initial power excursion and the subsequent behaviour of the core. Notably, SCRAM was intentionally not considered in these simulations to represent a bounding,

worst-case scenario, focusing solely on the inherent response of the core design to the reactivity insertion.

Initially, the control rods were positioned to maintain the core in a critical state and the highest-reactivity-worth control rod was assumed to be ejected. The simulations use an adaptive time step with a maximum of 1.0×10^{-3} seconds for the initial 1.0 s. A coarser time step of 0.02 s was subsequently used for the remaining time of the 3 s simulations.

2.2.2. REA Acceptance Criteria and Safety Limits

The consequences of these power excursions were evaluated against established safety criteria for REAs. An REA is classified as a Level 3a event within the Defense-in-Depth (DiD) framework and is considered a design-based accident. Therefore, many countries have established their own safety criteria. The OECD/NEA report [18] compares regulatory acceptance criteria across 12 member countries. Although criteria vary nationally, the primary safety objectives regarding REAs remain consistent: to prevent the loss of long-term core coolability and avoid damage to the reactor pressure boundary and core structures due to pressure wave generation. Notably, fuel cladding failure is generally not considered a safety concern (except in Germany). However, REA experimental and modelling efforts have focused extensively on fuel rod failure for several reasons:

- Fuel rod failure is a prerequisite for both the loss of coolable core geometry and the generation of substantial coolant pressure pulses. These complex phenomena exceed the simulation capabilities of standard transient analysis tools such as SIMULATE5-K.
- The mechanisms of fuel failure are more tractable to experimental and analytical investigation than core-wide cooling degradation and structure damage process.

Consequently, the most conservative design criterion is to prevent fuel damage entirely during an REA. To ensure fuel cladding integrity, two parameters are monitored against the fuel cladding thresholds [19]:

- Peak fuel pin enthalpy: The established safety limit requires the peak fuel enthalpy to remain below 418.4 kJ/kg (100 cal/g) for the radioactive state.
- Minimum departure from nucleate boiling ratio (MDNBR): Cladding failure is presumed if the local heat flux violates the DNB acceptance criterion. The minimum acceptance DNBR is 1.3, which is based on a statistical analysis with at least a 95% probability at a 95% confidence level.

The fuel pin enthalpies and MDNBR at HFP of the original core are displayed in Figure 3. The maximum fuel enthalpy at the MOC is 484.9 kJ/kg, exceeding the fuel failure limit by 15.9%. Therefore, the fuel cladding failed at the MOC.

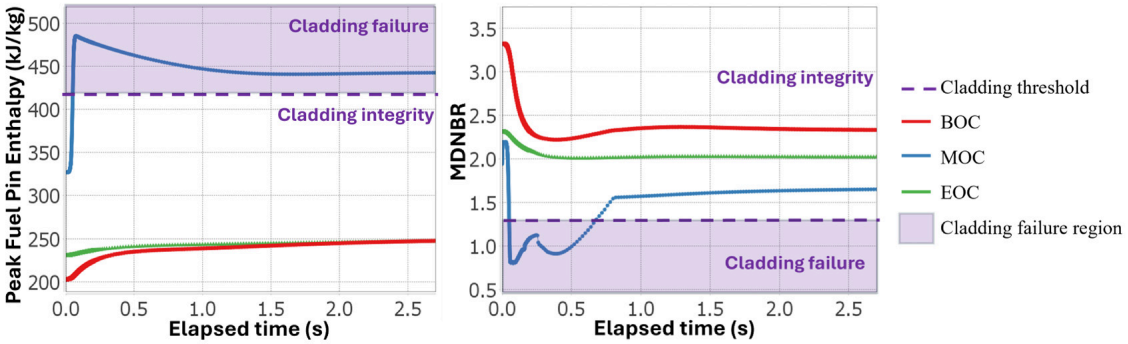

Figure 3. Fuel cladding integrity during rod ejection accident of the original equilibrium core.

This different safety phenomenon arises from the core's kinetic response to the inserted reactivity. To quantify the severity of the reactivity insertion, it is conventional to express the reactivity in dollars as $\rho(\$) = \frac{\rho_{rod}}{\beta_{eff}}$, where ρ_{rod} is the worth of the ejected control rod and β_{eff} is the effective delayed neutron fraction. When the normalized reactivity $\rho(\$)$ remains below 1, the reactor is in a delayed supercritical state where the power change is primarily governed by the delayed neutrons, leading to a relatively slow and manageable power increase. If $\rho(\$)$ exceeds 1, the reactor promptly becomes supercritical and the power increases exponentially [20,21]. As displayed in Figure 4, the values of $\rho(\$)$ are below 1.0 at the BOC/EOC but larger than 1.0 at the MOC. The large inserted reactivity at the MOC induces a pronounced power surge (see Figure 5), which, in turn, deposits substantial energy in fuel, resulting in the excessively high fuel enthalpy presented in Figure 3.

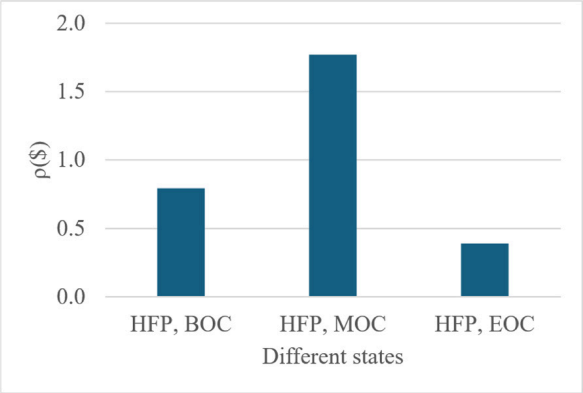

Figure 4. Normalized ejected control rod worths at different states for previous equilibrium core design.

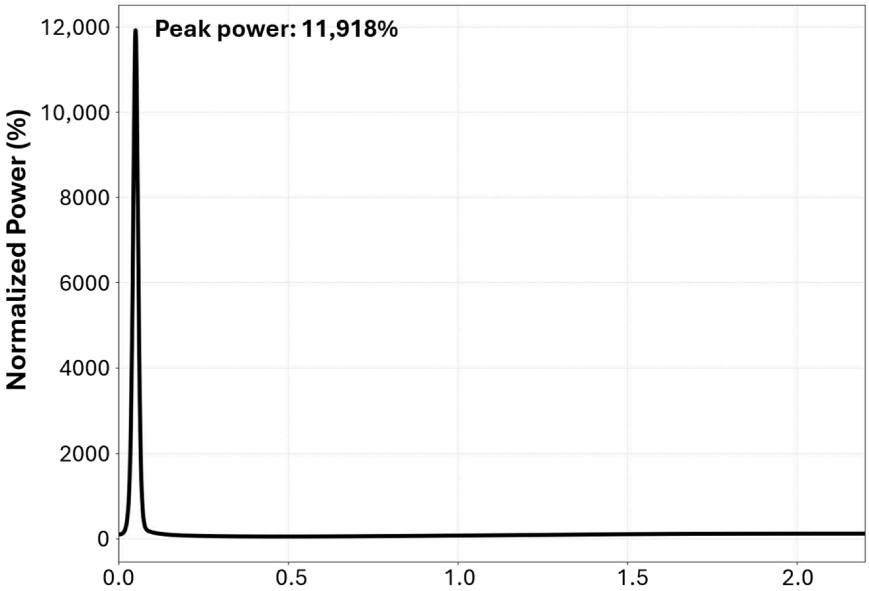

Figure 5. Power spike during rod ejection accident at HFP MOC of the original equilibrium core.

Therefore, to avoid the safety risks during an REA, the core design must ensure that the normalized reactivity worth of the ejected control rod is near or below 1$, preventing the uncontrollable rapid supercriticality.

3. Strategies to Optimize the Core Design

As discussed, to improve the safety margins during an REA, normalized reactivity must not exceed 1. Since β_{eff} is constant in each state, reducing the control rod worth was

necessary. Consequently, two solutions were proposed. Based on these two solutions, the optimization process was re-conducted by the in-house tool CoreOptimizer [10] integrated with CASMO5 and SIMULATE5, which will be shortly described in Section 3.2. The capabilities of CASMO5 and SIMULATE5 for this core have been verified in [22].

3.1. Two Solutions to Decrease the Individual Control Rod Worth

Guided by the understanding that control rod worth is influenced by several factors [23] such as rod material, rod location, fuel and gadolinium distribution in adjacent assemblies, and shadowing/anti-shadowing effects [24] between rods, the present paper proposes two strategies to mitigate the excessive CR worth in single FA compared with the previous core design:

- A hybrid control rod configuration was adopted, replacing 12 Ag-In-Cd rods with stainless steel in assemblies containing regulating banks.
- The refuelling loading pattern was reorganized to prevent fresh fuel clustering, which inherently limits the local power and reactivity peaks.

The reasons are explained in detail as follows.

3.1.1. Control Rod Configuration in Fuel Assembly

The selection of CR material is primarily based on their neutron absorption capability. Silver–indium–cadmium (AIC) alloy, typically composed of 80% Ag, 15% In and 5% Cd, is a widely-used CR material in PWRs because the primary isotopes in AIC (Ag-109, Ag-107, In-115) possess large neutron absorption cross-sections in the thermal neutron energy range (see Figure 6). Furthermore, AIC exhibits multiple absorption resonances across intermediate energies, allowing it to effectively absorb neutrons even before they are fully thermalized.

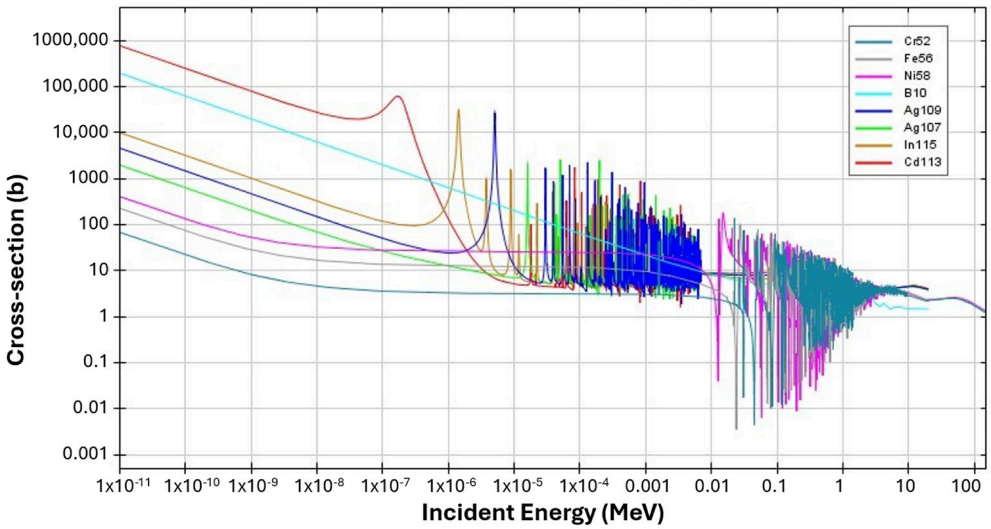

Figure 6. Energy dependence of the microscopic cross section of the isotopes of selected control rod materials. Source: JANIS 4.1 (Java-based Nuclear Data Information Software); ENDF/B-VII.1.

In contrast, stainless steel (SS) is characterized by a much smaller neutron absorption cross section. Its main constituents (Cr-52, Fe-56 and Ni-58) show much smaller cross-sections across the thermal and lower energy ranges compared with AIC's isotopes.

In the regulating banks of previous designs [16], each fuel assembly contained 24 guide tubes intended either entirely for AIC rods or entirely for SS rods. The FAs comprised entirely of SS lacked the total worth necessary for an adequate total core-wise shutdown margin, whereas the AIC-only FAs generated excessively high individual CR worths. To

achieve an intermediate neutron absorption ability in each assembly while providing enough excess reactivity control for the whole core, a hybrid CR configuration was adopted in regulating banks, inspired by AP1000 technology [25]. As illustrated in Figure 7, each assembly incorporates 12 AIC rods and 12 SS rods in the regulating banks of the optimized core. To maintain a sufficient shutdown margin, the safety banks utilize the configuration with 24 AIC rods.

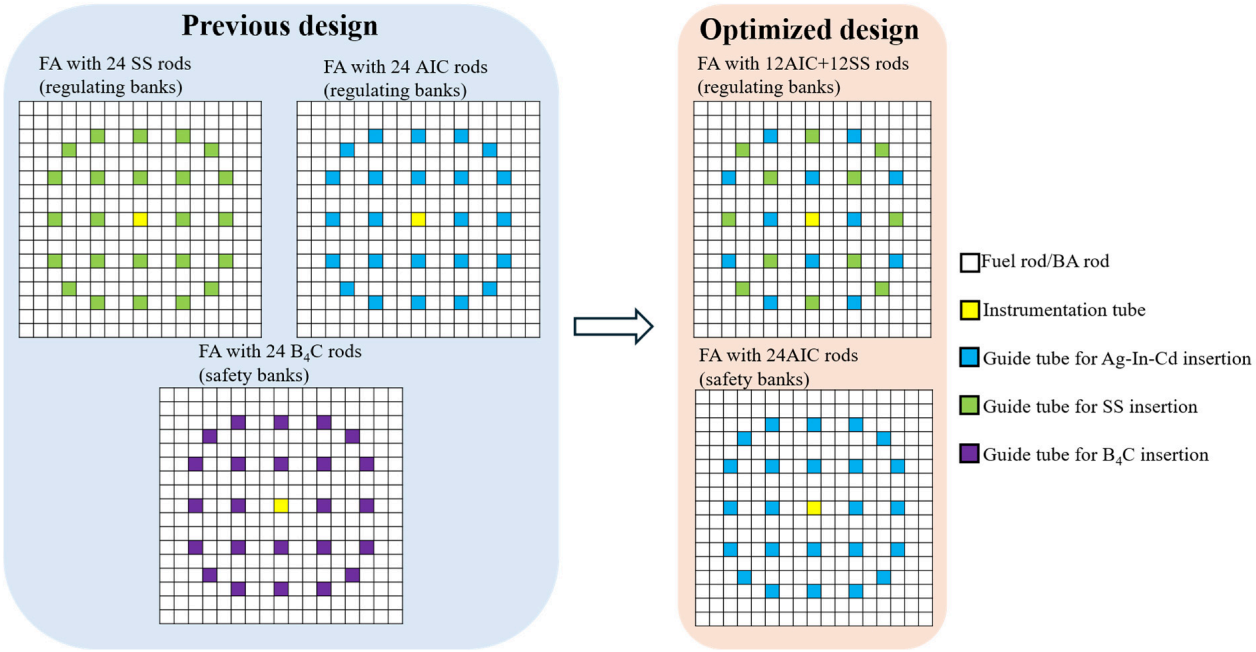

Figure 7. Control rod guide tubes in one fuel assembly with the material modification.

3.1.2. Refuelling Loading Pattern Reorganization

Figure 8 depicts the previous and optimized refueling loading patterns, where each FA's position is identified by a serial number representing its current (Cycle N) column and row. For cycle N, the serial numbers written on the burned FAs indicate their previous locations in the preceding cycle (Cycle N-1). Similar to the original designs, two-batch and multi-radial-zones strategies were applied.

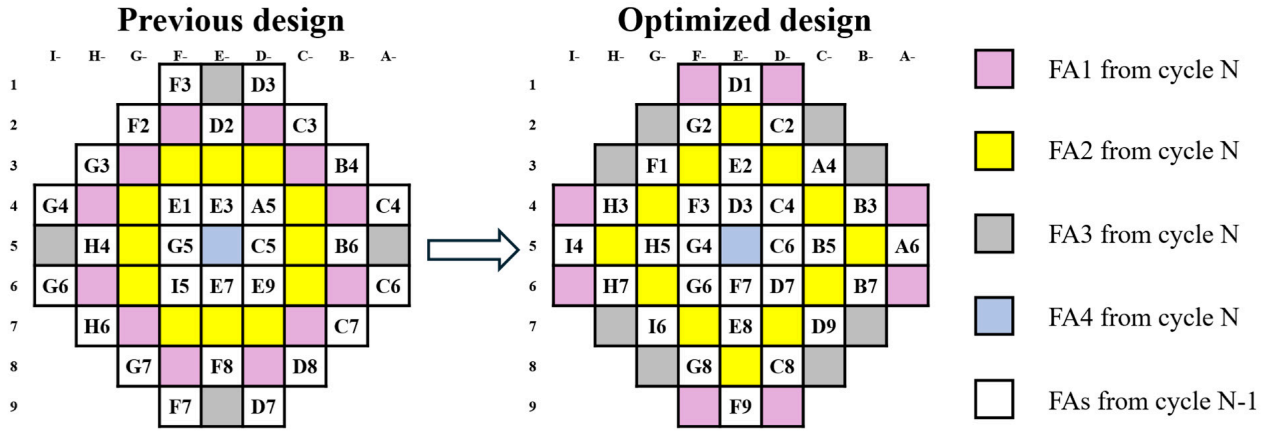

Figure 8. Optimized refuelling loading pattern to reach the equilibrium cycle core.

In the previous core design, several fresh FAs were positioned adjacently, resulting in high local excess reactivity, thereby necessitating a high local CR worth. To mitigate these requirements, the optimized refuelling loading pattern ensures that no fresh FAs are placed in adjacent positions, avoiding localized reactivity peaks.

3.2. Optimization Process Based on the Two Solutions

Based on these two solutions, the optimization process was re-conducted by the in-house tool CoreOptimizer. This tool integrates the entire process of generating cross-section via CASMO5 and performing 3D core simulation via SIMULATE5, handling the aspects from input generation, codes execution, and output data extraction.

This study followed the same optimization process detailed in [16]. This approach is briefly summarized as follows: With a set of fixed core design specifications, a brute-force search was employed to explore the large variable space. The variables considered in this search were fuel enrichment, number of BA rods per assembly, and the Gd_2O_3 concentration in BA rods (BA loading). Following the two changes to the core specification, the efficiency of CoreOptimizer in facilitating the re-optimization was confirmed by quantitatively comparing the time required using CoreOptimizer versus a manual approach.

3.2.1. Constrains

The constraints are described in [16], including the total FA number of 57, pin geometry, and operating conditions.

The optimized designs offer more options of BA configurations in FA, utilizing different numbers of BA rods (16, 24 and 32 rods per FA according to [8,26]). Figure 9 shows the FA designs characterized by the same CR-positions with varying number of BA rod number ranging from 12 to 40 considered in this investigation and the optimized BA numbers were searched for in the subsequent core design process.

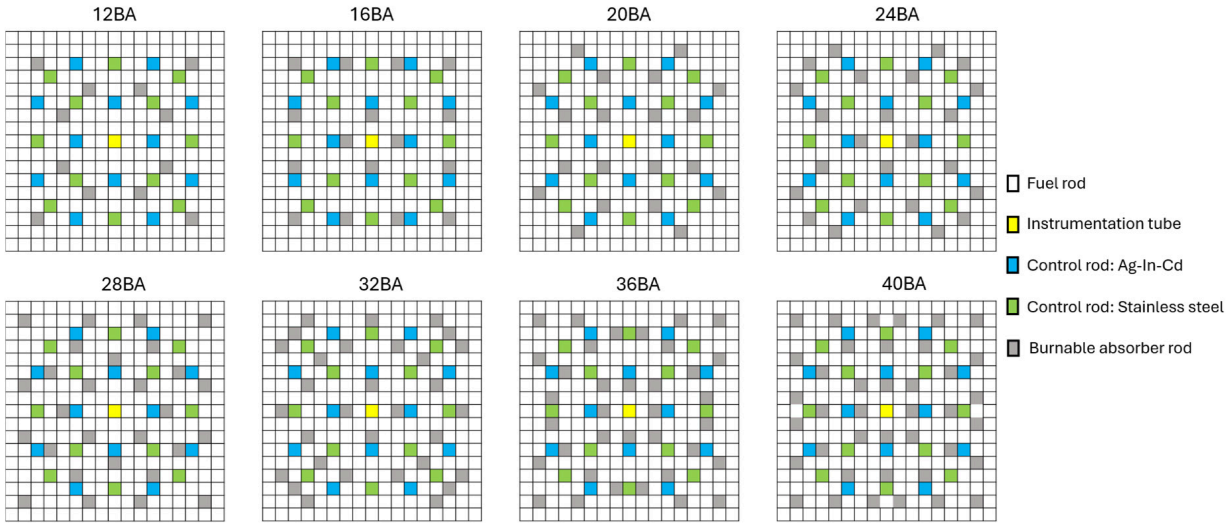

Figure 9. Radial arrangements of the FAs with various BA rods.

3.2.2. Variable Search Space for the Optimized Equilibrium Cycle Core

After certain parameters were constrained, the remaining design variables included the control rod layout, fuel enrichment, burnable absorber (BA) rod number per FA and BA loading.

To find the good combinations of the latter three parameters, a brute-force search approach was employed. This method tested numerous combinations of these parameters to identify the optimal combination for the equilibrium cycle. The control rod layout was proposed during this variable search process.

The combinations of fuel assembly parameters were assigned based on the refuelling loading pattern in Figure 8: FA1 (pink) and FA3 (grey) are primarily located in the outer-region positions of the core. They are characterized by higher enrichment with fewer BA rods. This strategy compensates for the lower neutron flux in peripheral regions, ensuring relatively uniform power distribution. FA2 (yellow) occupies the inner region. These FAs are assigned lower enrichment and additional BA concentration to control the power peak in the high-flux inner regions. The central assembly FA4 (blue) is assigned the lowest enrichment to minimize the central power peak.

Therefore, the range of variables for the four FAs are defined with specific intervals, as shown in Table 1. This systematic combination results in 30 lattice models. As the core consists of four fresh FA types, the total number of core configurations was calculated as the product of these combinations, yielding 3456 configurations.

Table 1. The combinations of fuel assemblies at equilibrium for selection.

Fresh FA Types	Enrichment (%)	BA Rods per FA	BA Loading (%)	Combinations
FA1	4.8, 4.95	16, 20, 24	4, 8	12
FA2	4.0, 4.2, 4.4	28, 32, 36, 40	10	12
FA3	4.8, 4.95	16, 20, 24	4, 8	12
FA4	1.8	20, 24	8	2

3.2.3. Brief Description of the Variable Search Process

The detailed process for the equilibrium cycle was described in [16], which is achieved by multi-stage selections:

(1) All-Rod-Out (ARO) Search

The design process began with a search under ARO conditions. The ARO simulations were repeated for multiple cycles with a fixed cycle length and the ARO equilibrium was reached by cycle 4 when the k_{eff} difference between adjacent cycles was less than 243 pcm. In addition to guiding the CR layout, this step established the ARO equilibrium state, which guided the determination of the CR radial layout.

(2) Control rod layout determination

CoreOptimizer provides the capability for iterative search repetitions, allowing for evaluation of various CR layouts when the optimal configuration is uncertain. Multiple CR layouts were simulated under critical conditions for ARO equilibrium cycle configurations, which was reached after three extra cycles [16], each fixed at 21 GWd/t burnup.

All configurations were filtered by CoreOptimizer against the operating safety criteria [16,27], collected from IAEA [28], U.S. NRC [29], and KTA [30] and detailed as follows:

- $F_q \leq 3.26$;
- $F_{\Delta H} \leq 1.62$;
- $-0.4 \leq$ axial offset ≤ 0.4;
- FTC < 0;
- MTC < 0.

Following the application of these constraints, some CR layouts retained no configurations, indicating their unsuitability for this core design. Ultimately, two control rods were selected for further comparison, as illustrated in Figure 10. Each layout comprises four regulating banks (R1–R4) and two safety banks (S1, S2). The regulating banks were equipped with hybrid control rods (12 Ag-In-Cd + 12 stainless steel) designed to mitigate axial power peaking (see Figure 7). The safety banks, conversely, consisted solely of Ag-In-Cd rods to ensure a sufficient shutdown margin.

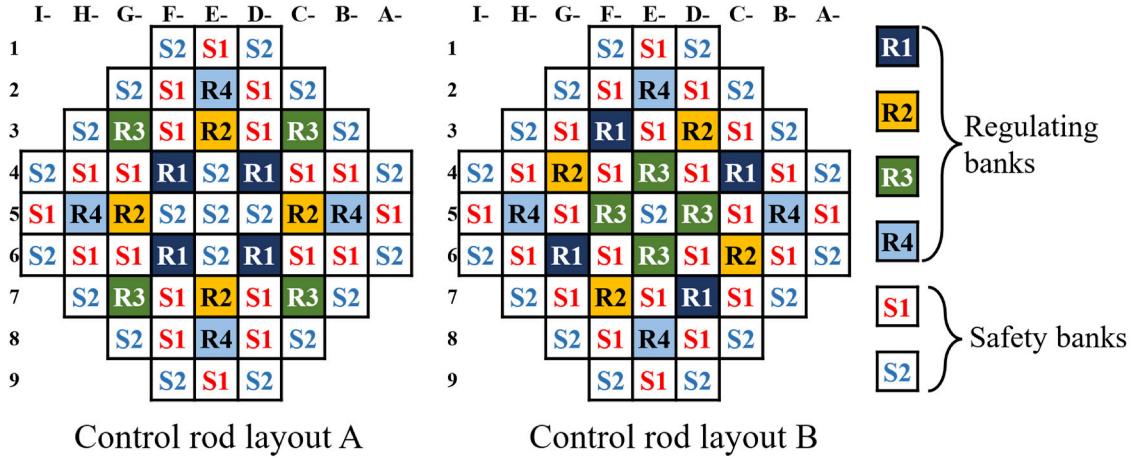

Figure 10. Two control rod layouts for the optimized equilibrium simulations.

(3) Critical Search

The determined control rod movement sequences were applied to all core configurations. The simulations then proceeded under critical conditions for multiple extra cycles, where each cycle had a fixed cycle length of 21 GWd/t, a consistent refuelling strategy, and consistent new fuel assemblies as last cycle.

3.2.4. Parameters Combinations of the Optimized Core Designs

Among the configurations that satisfied all the safety criteria, those that exhibited the minimum peak F_q throughout the cycle were selected as the optimized equilibrium cycle core configurations for each control rod layout, as listed in Table 2.

Table 2. Optimized core configurations for equilibrium cycle.

Control Rod Layouts	FAs	Fuel Enrichment (%)	BA Number per FA	BA Loading (%)
CR layout A	FA1	4.8	24	8
	FA2	4.2	32	10
	FA3	4.8	24	8
	FA4	1.8	20	8
CR layout B	FA1	4.8	24	8
	FA2	4.2	28	10
	FA3	4.8	24	8
	FA4	1.8	20	8

3.3. Efficiency Improvement by In-House Tool CoreOptimizer

Any modification to the fuel assembly configuration necessitates regenerating cross sections via CASMO5 and re-conducting core simulations by SIMULATE5. This is where CoreOptimizer plays a critical role. For example, CoreOptimizer integrates with SIMULATE5, managing input templates for the equilibrium cycle with a new refuelling loading

pattern. Once templates are modified with updated configurations, the search process can be restarted. With CoreOptimizer, the user initiates the process with a single click per cycle. The automation enables all simulations to be conducted overnight and drastically cuts down the time required for repetitive simulations. For instance, as shown in Table 3, the equilibrium cycle search process is accelerated using CoreOptimizer under the following approximated conditions:

- Writing an input file for SIMULATE5: 3 min;
- Start and execution: 1 min;
- Burnup simulation per cycle: 5 min;
- Number of parallel simulations: 6;
- Manual working hour: 8 h/day;
- Program working hour: 24 h/day.

Table 3. Comparison of consumed time between manual effort and CoreOptimizer.

Method	Time per Cycle	Working Time per Cycle	Total Time (Cycle 2–7)
Manual Effort	$= \frac{(3+1+5)\times 3456}{6} = 5184$ min	$= \frac{5184 \text{ min}}{8\ \text{h/day}} \approx 10.8$ days	$= 10.8 \text{ days} \times 6 \approx 65$ days
CoreOptimizer	$= \frac{5\times 3456}{6} = 2880$ min	$= \frac{2880 \text{ min}}{24\ \text{h/day}} = 2$ days	$= 2 \times 6 = 12$ days

By using CoreOptimizer, the equilibrium cycle search process is shortened by 53 days—a 81.5% reduction compared with manual efforts.

4. Analysis of the Optimized Cores

The optimal equilibrium core adopted the refuelling loading pattern shown in Figure 8, and the two radial arrangements of CR banks (CR-A and CR-B) are depicted in Figure 10. The optimized core configurations are listed in Table 2. The control rod axial positions throughout the cycles are displayed in Appendix A.

This section presents a comprehensive analysis of the optimized core designs with two control rod layouts at equilibrium cycle. First, the analysis briefly compared the key neutronics and safety parameters for the two control rod layouts under hot full power (HFP) normal operational conditions. This step confirmed that the optimized cores consistently met all necessary safety criteria throughout their operational cycles. Furthermore, the shutdown margins with single failure under the cold zero power (CZP) scenario were estimated to confirm the optimized control rod designs provide sufficient shutdown capabilities. Subsequently, the individual normalized control rod worth was analyzed under HFP and HZP conditions; the layout with the smaller peak normalized CR worth was selected for the following REA simulation. By investigating transient behaviour and fuel cladding integrity, the analysis demonstrated the inherent safety capability of the optimized core.

4.1. Comparison of Key Safety Parameters During Normal Operation

The key safety parameters during normal operation were summarized in [16], mainly including the 3D and 2D pin power factors, power axial offset, fuel temperature coefficient and moderator temperature coefficient. These parameters served as the filtering constraints during the optimization process. As displayed in Figure 11 and Table 4, all of the safety parameters demonstrate sufficient safety margins throughout the operational cycles for both control rod layouts.

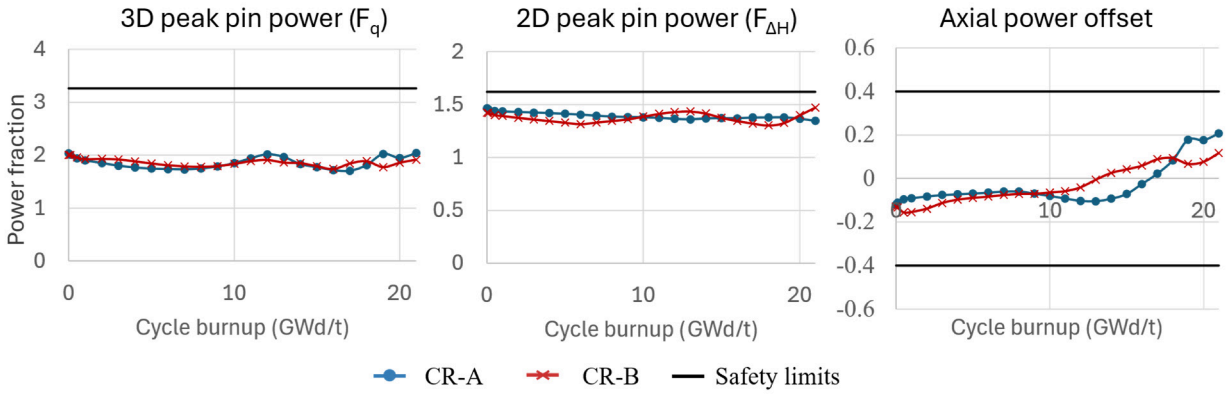

Figure 11. 3D pin power factors, 2D pin power factors and power axial offsets throughout the optimized equilibrium cycles.

Table 4. Reactivity temperature coefficients at BOC/MOC/EOC of equilibrium cycle.

Temperature Coefficients	CR Layout	BOC	MOC	EOC
Fuel temperature coefficient (pcm/K)	CR-A	−1.48	−1.48	−1.55
	CR-B	−1.48	−1.50	−1.55
Moderator temperature coefficient (pcm/K)	CR-A	−41.88	−40.82	−44.18
	CR-B	−42.11	−40.48	−41.90

4.2. Estimation of the Cold Shutdown Margin with Single Failure for BOC, MOC, and EOC

As discussed in Section 1, the designed core must provide an adequate shutdown margin with one stuck CR after the control rod optimization. To ensure conservative safety margins, the highest-worth control rod is assumed to be fully withdrawn while all others fully inserted at cold conditions. According to the KTA safety criteria, the cold shutdown margin (CSDM) with a single failure must be at least 1000 pcm under this restrictive assumption [30].

Table 5 summarizes the cold shutdown margin (CSDM) with a single failure during burnup for these two CR layouts. The results confirm that the optimized control rod designs provide sufficient shutdown margins under the most conservative condition.

Table 5. Cold shutdown margin with single failure during burnup at equilibrium cycles.

States / Reactivities	CR-A			CR-B		
	BOC	MOC	EOC	BOC	MOC	EOC
CSDM with single failure (pcm)	5039	7860	9682	4403	7762	11,601

4.3. Comparison of Normalized Ejected Reactivities Under HFP/HZP Conditions

Figures 12 and 13 summarize the differences between the highest ρ_{rod} and the β_{eff} under HFP/HZP conditions at the BOC/MOC/EOC for CR-A and CR-B. The location of highest ρ_{rod} in different states can be found in Appendix B. For the CR-A layout, the $\rho(\$)$ values are smaller than 1.0 at the HFP EOC and HZP BOC/MOC, while bigger than 1.0 at the HFP BOC/MOC, with a peak value of 1.60$ at the HFP BOC. For the CR-B layout, the $\rho(\$)$ values are confined to a very small range close to 1.0 across all states, peaking at 1.28$ at the HZP EOC.

In summary, the optimization efforts successfully reduced the maximum $\rho(\$)$ values for equilibrium cycles compared with the original core designs (illustrated in Figure 4), showing 12% and 29% reductions in the peak normalized reactivities for CR-A and CR-B.

According to the discussion in Section 2.2.2, limiting the ejected rod worth ρ($) to smaller or close to 1$ can avoid the safety risks during an REA. Based on the steady-state analysis of ρ($), the CR-B layout demonstrates a marginally safer performance than CR-A. Therefore, the CR-B layout was chosen to conduct the rod ejection accident simulations.

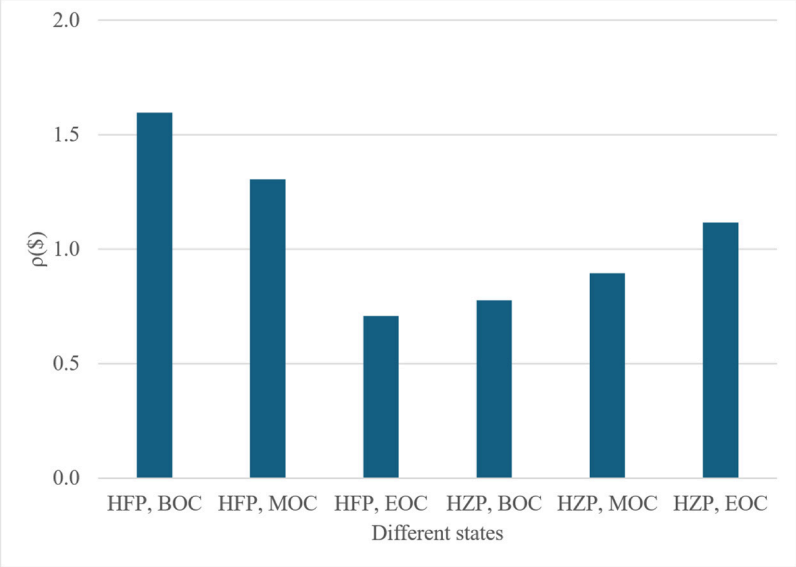

Figure 12. The highest control rod worth and delayed neutron fractions at different states for CR-A at equilibrium.

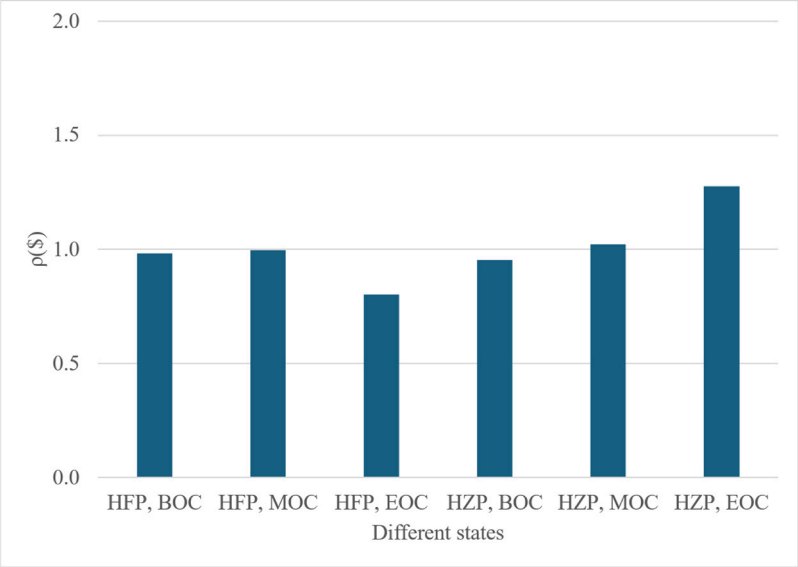

Figure 13. The highest control rod worth and delayed neutron fractions at different states for CR-B at equilibrium.

4.4. Transient Behaviour During REA in the Optimized Equilibrium Core

Using the same assumptions in Section 2.2.1, the REAs are simulated under both hot full power (HFP) and hot zero power (HZP) conditions, as summarized in Table 6.

This section provides the results of a comprehensive transient analysis of the global power excursions and their underlying mechanisms for the optimized equilibrium core. Additionally, a fuel integrity evaluation was conducted to assess the safety margins during the REA.

Table 6. Initial conditions of the rod ejection accident.

Parameters	HFP	HZP
Thermal power	330 MW	1.0×10^{-4}
Coolant flow rate	2006.4 kg/s	2006.4 kg/s
Pressure	15.0 MPa	15.0 MPa
Temperature	Coolant inlet temperature: 296 °C	Average temperature of fuel and coolant: 296 °C

4.4.1. Global Power Response During REA

Figure 14 displays the global power responses at the BOC/MOC/EOC under HFP and HZP conditions in the optimized equilibrium core. The highest peak power among all the scenarios occurs at the HZP EOC, with a peak power of 1264%, which is 89% less than the peak power in the original core.

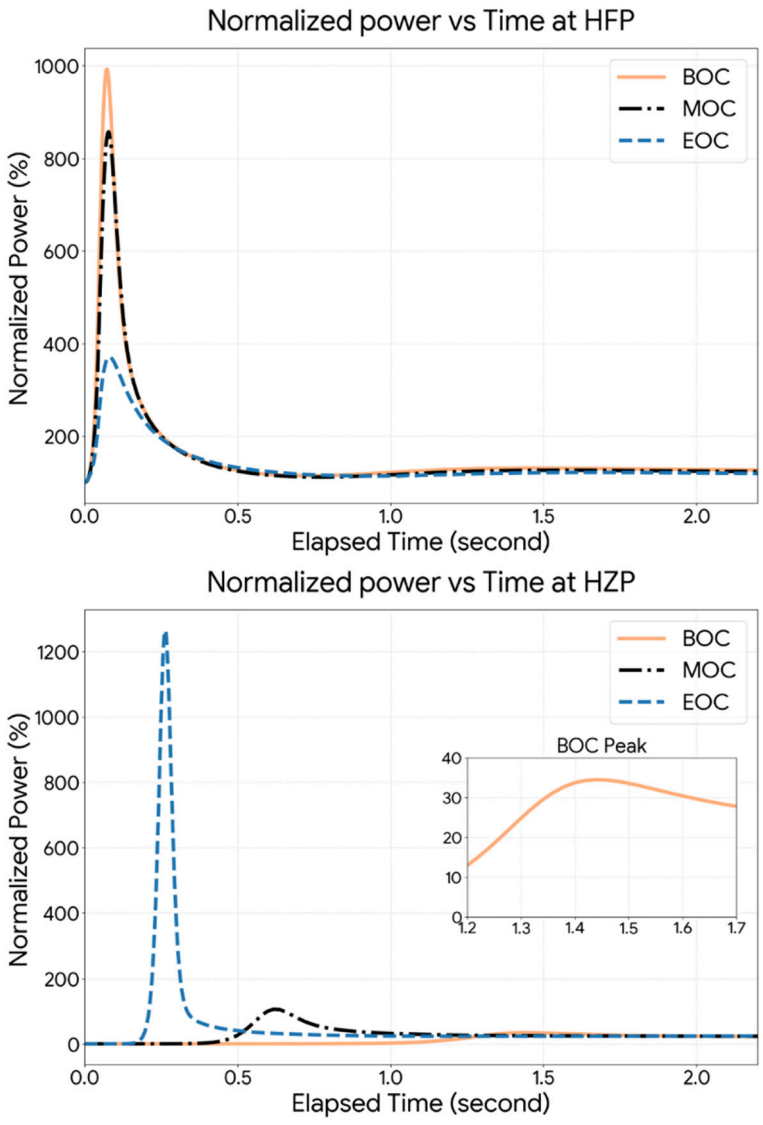

Figure 14. Normalized power variation during REA under HFP and HZP conditions.

The results demonstrate that the transient behaviour is highly sensitive to the initial state and the magnitude of the inserted normalized reactivity ρ($):

- HFP scenarios: Power rises immediately after rod ejection across all burnup stages. A larger ρ($) directly results in a larger power peak, with peaks reaching at approximately the same time for the BOC, MOC and EOC.
- HZP scenarios: The power rise is notably delayed compared with HFP scenarios. A larger ρ($) not only increases the power peak magnitude but also results in an earlier power rise.

4.4.2. Comparison of Feedback Mechanisms Between HFP and HZP Conditions at EOC

To investigate the underlaying mechanisms governing different power excursions during an REA, a comprehensive comparison between the HFP EOC and HZP EOC was performed. The basic governing equations during an REA are the point reactor kinetics (PRK) equations, given in (1) and (2):

$$\frac{dn(t)}{dt} = \frac{\rho(t) - \beta_{eff}}{\Lambda} n(t) + \sum_{i=1}^{6} \lambda_i C_i(t) \quad (1)$$

$$\frac{dC_i(t)}{dt} = \frac{\beta_i}{\Lambda} n(t) - \lambda_i C_i(t) (i = 1, 2, \ldots, 6) \quad (2)$$

where $n(t)$ represents the change in the neutron density in time, which is proportional to the power, $\rho(t)$ is the ejected control rod reactivity, β_i is the fraction of the i-th delayed neutron group and β_{eff} is the effective delayed neutron fraction, Λ is the neutron generation time and $C_i(t)$ represents the concentration of the i-th delayed neutron precursor group. The key kinetics parameters and ejected control rod reactivity are summarized in Table 7.

Table 7. Key kinetics parameters and ejected rod reactivity for HFP MOC and HZP MOC.

	HFP EOC	**HZP EOC**
Effective delayed neutron fraction β_{eff}	5.19×10^{-3}	5.27×10^{-3}
Neutron lifetime Λ (s)	2.25×10^{-5}	2.17×10^{-5}
Ejected rod reactivity ($)	0.76	1.26

The reactivity feedback mechanisms are collected in Figure 15. Based on these observations, the underlying mechanisms driving the transient power excursion are discussed below.

- HFP EOC State

Because the initial power is 100%, the fuel temperature increases instantaneously, leading to the Doppler feedback response at 0.07 s. This prompt feedback causes the total reactivity to begin to decline simultaneously. However, it is observed that the turnaround point of the power occurs at 0.09 s, which is later than that of reactivity. The physical mechanism underlying this delay can be derived from Equation (1) under the condition $\frac{dn(t)}{dt} = 0$, yielding Equation (3):

$$\rho(t) = \beta_{eff} - \frac{\Lambda \cdot \sum_{i=1}^{6} \lambda_i C_i(t)}{n(t)} \quad (3)$$

Since the second term on the right-hand side $\frac{\Lambda \cdot \sum_{i=1}^{6} \lambda_i C_i(t)}{n(t)}$ is positive, the reactivity at the power turnaround point must satisfy $\rho(t) < \beta_{eff}$.

While the MTC contributes to long-term stabilization, it does not contribute to the power pulse due to the inherent time constant of heat transfer from the fuel to the coolant.

- HZP EOC State

For a step reactivity insertion, the analytical response of the neutron population can be approximated from (1) and (4), which is applicable before the core's negative feedback mechanisms are activated.

$$n(t) = n(0)\left(\frac{\beta_{eff}}{\beta_{eff}-\rho}e^{\frac{\rho\cdot\lambda}{\beta_{eff}-\rho}t} - \frac{\rho}{\beta_{eff}-\rho}e^{\frac{\rho-\beta_{eff}}{\Lambda}t}\right) \quad (4)$$

Because the initial power is set to 10^{-4} of nominal power, the power remains numerically small during the initial phase of the transient according to (4), maintaining a constant fuel temperature until 0.20 s. Once the power rises sufficiently and the fuel is heated up, Doppler feedback is triggered at 0.22 s, resulting in a decline in total reactivity from its peak plateau. Subsequently, the power excursion is terminated at 0.26 s when the reactivity satisfies Equation (3). Similar to HFP scenarios, the MTC begins to manifest at approximately 0.33 s after the primary power pulse.

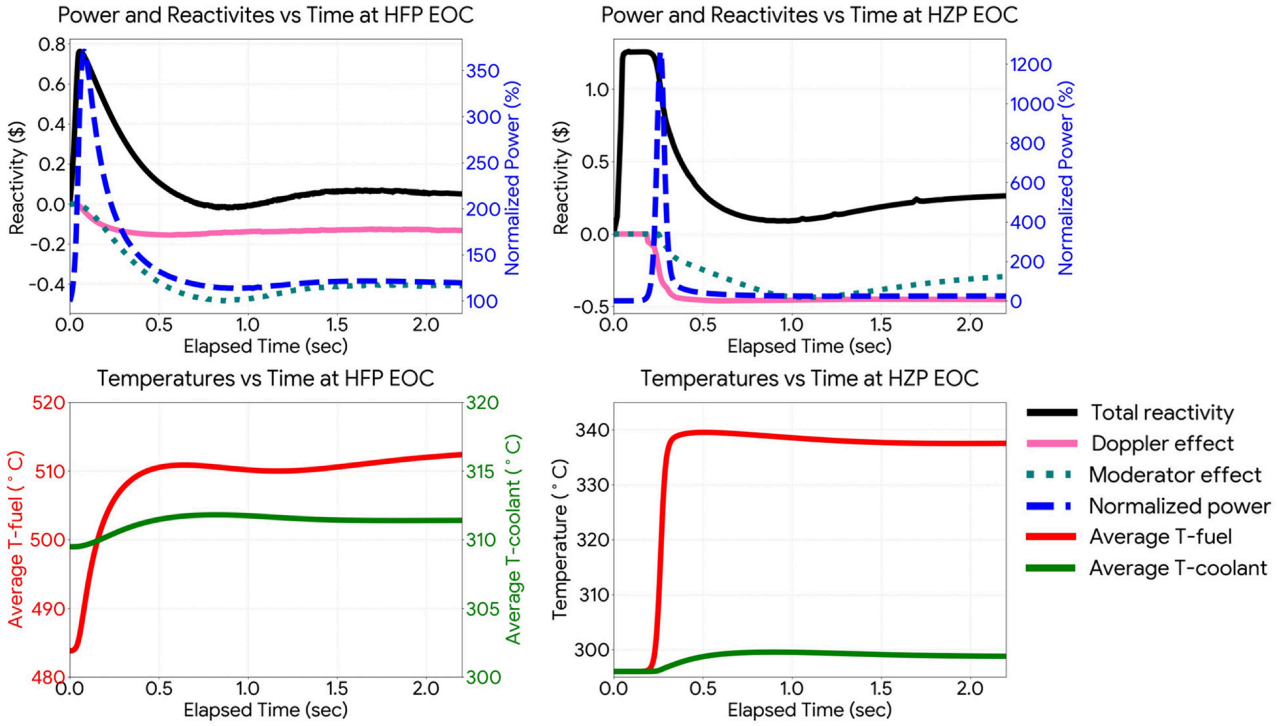

Figure 15. Reactivity feedback mechanisms and temperature variations during REA at HFP EOC and HZP EOC.

4.4.3. Fuel Cladding Integrity Evaluation

As discussed in Section 2.2.2, fuel cladding integrity is considered maintained as long as the fuel enthalpy remains below its maximum limit of 418.4 kJ/kg and the DNBR stays above its minimum limit of 1.3.

As depicted in Figure 16, for all the HFP and HZP scenarios, the fuel enthalpies and the MDNBRs remain well within their respective safety limits. Therefore, all the fuel cladding integrities are maintained in the optimized equilibrium core. This demonstrates a superior safety margin to the previous core design.

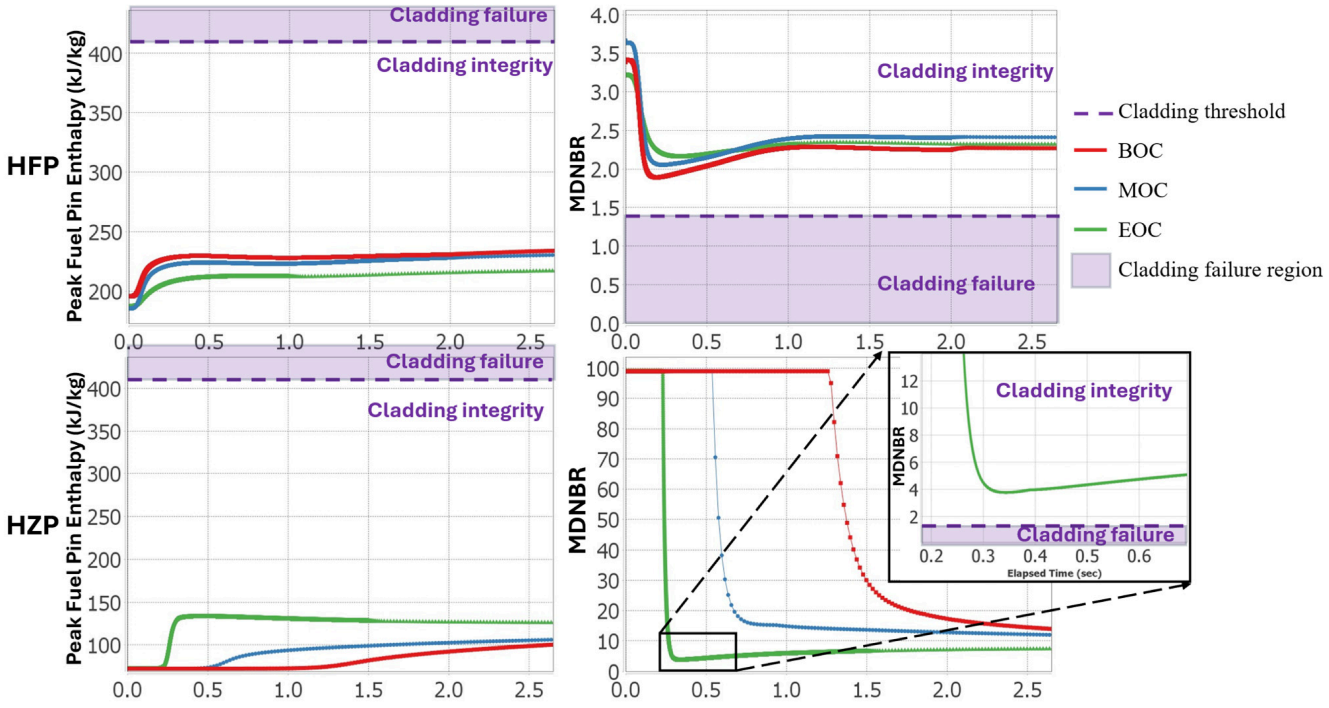

Figure 16. Evaluation of fuel cladding integrity under HFP and HZP conditions.

5. Conclusions and Outlooks

Based on the new fuel assembly configuration with hybrid control rod and the re-arrangement of the refuelling loading pattern, the equilibrium cycle core was re-designed using the CoreOptimizer to automate the input file generation, execution, and output data extraction of CASMO5 and SIMULATE5. In the optimized equilibrium core, the safety characteristics over the cycle are well below the safety limits and the control rods provide sufficient shutdown margins. Most importantly, the optimized core features reduce the individual control rod worth, which lowers the global power peak, thereby ensuring that the fuel cladding integrity is maintained during an REA.

The previous research [16] and this study establish the primary process for core design and optimization of an SBF SMR. Future efforts may focus on other methodologies and techniques within this process to further refine the refuelling strategies and control rod radial layouts, thereby enhancing the fuel utilization.

Author Contributions: Conceptualization, V.H.S.-E. and Y.S.; methodology, Y.S.; software, Y.S.; formal analysis, Y.S.; investigation, Y.S.; resources, Y.S.; data curation, Y.S.; writing—original draft preparation, Y.S.; writing—review and editing, V.H.S.-E.; visualization, Y.S.; supervision, V.H.S.-E. All authors have read and agreed to the published version of the manuscript.

Funding: This research received no external funding.

Data Availability Statement: Data available on request due to institutional policy restrictions.

Acknowledgments: My sincere thanks go to Luigi Mercatali, G. H. Zavala and K. L. Zhang. Their discussions and feedback enabled the progress of this research.

Conflicts of Interest: The authors declare no conflicts of interest.

Abbreviations

The following abbreviations are used in this manuscript:

AIC	Silver–indium–cadmium
BA	Burnable absorber
BA per FA	Burnable absorber rod number per fuel assembly
B_4C	Boron carbide
BOC	Beginning of cycle
CR	Control rod
ENR	Fuel enrichment
EOC	End of cycle
FA	Fuel assembly
FTC	Fuel temperature coefficient
HFP	Hot full power
HZP	Hot zero power
MDNBR	Minimum departure from nucleate boiling ratio
MOC	Middle of cycle
MTC	Moderator temperature coefficient
PWR	Pressurized water reactor
REA	Rod ejection accident
SBF	Soluble-boron-free
SS	Stainless steel
WC-SMR	Water-cooled small modular reactor
β_{eff}	Effective delayed neutron fraction
ρ($)	Normalized ejected control rod worth

Appendix A

The control rod positions throughout the optimized equilibrium cycles with the two control rod layouts are illustrated in Figure A1.

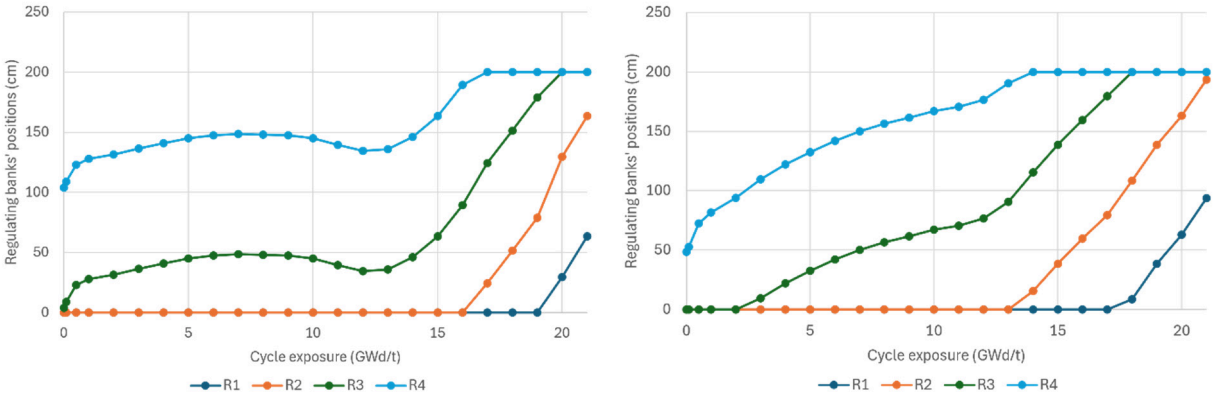

(**a**) Regulating banks' positions with CR-A (**b**) Regulating banks' positions with CR-B

Figure A1. Regulating control rod banks' positions throughout the cycle.

Appendix B

In the optimized equilibrium cycle core, the specific initial control rod positions during an REA in different states (HFP/HZP and the BOC/MOC/EOC) are provided in Figures A2 and A3. The control rod assembly with the highest reactivity worth for ejection is marked with red circles in each state.

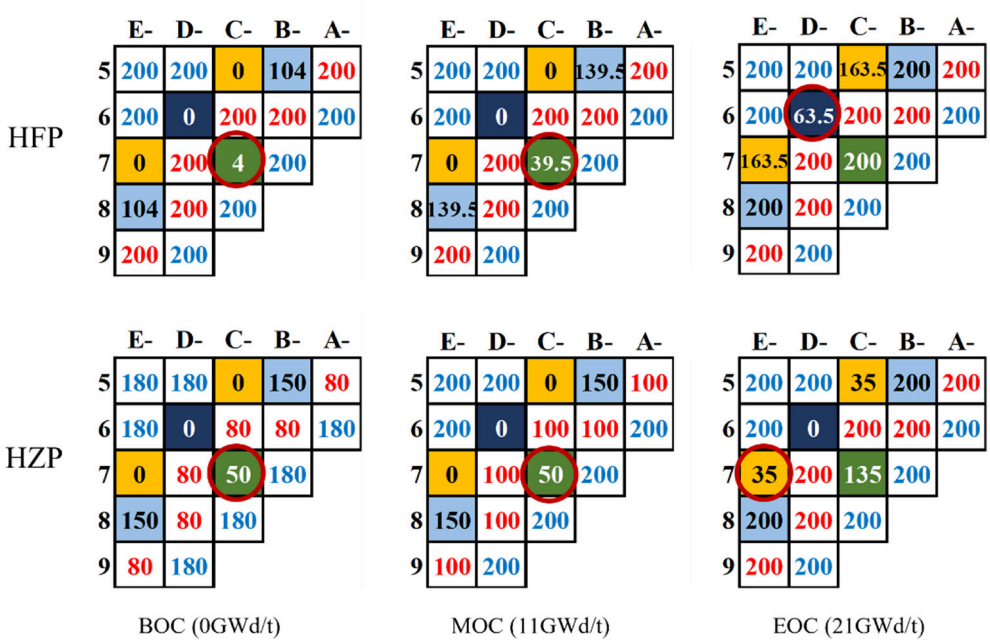

Figure A2. Locations of highest control rod worth of CR-A during optimized equilibrium cycle.

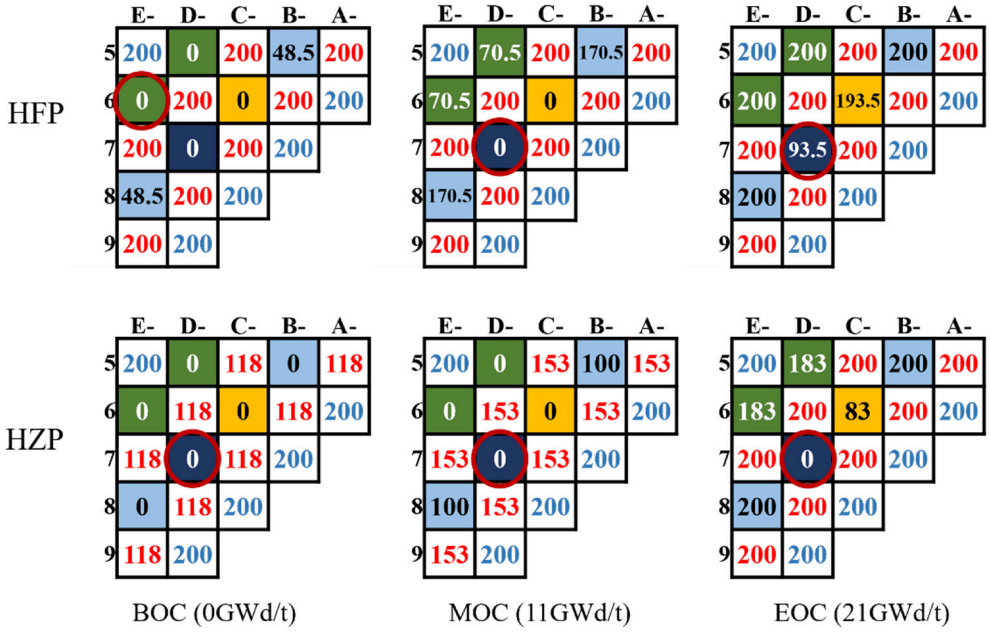

Figure A3. Locations of highest control rod worth of CR-B during optimized equilibrium cycle.

References

1. Qu, Y. Development and Construction of ACP100. In Proceedings of the Interregional Workshop on Generic User Requirements and Criteria for SMRs (NHSI Topic 1), Sanya, China, 4–8 September 2023.
2. IAEA. Small Modular Reactors: Advances in SMR Developments. In Proceedings of the International Conference on Small Modular Reactors and Their Applications, Vienna, Austria, 21–25 October 2024.
3. Rolls-Royce-SMR. *Environment, Safety, Security and Safeguards Case Version 2, Tier 1, Chapter 4: Reactor (Fuel and Core)*; Rolls-Royce-SMR: Manchester, UK, 2024.
4. Tagirova, T. *Status of RITM Technology Development and Deployment*; ROSATOM: Moscow, Russia, 2025.
5. Leppänen, J.; Valtavirta, V.; Tuominen, R.; Rintala, A.; Lauranto, U. A Finnish district heating reactor: Neutronics design and fuel cycle simulations. In Proceedings of the International Conference on Nuclear Engineering, Online, 4–6 August 2021.
6. Kang, H.; Lee, B.J.; Lim, S.G. Light water SMR development status in Korea. *Nucl. Eng. Des.* **2024**, *419*, 112966. [CrossRef]

7. Vuiart, R.; Eustache, A.; Eveillard, S.; Prulhière, G. PRATIC: A soluble-boron-free, pressurized water cooled, SMR core benchmark. *Nucl. Sci. Technol.* **2024**, *10*, 25.
8. Alzaben, Y.I. Neutronics and Thermal-Hydraulics Safety Related Investigations of an Innovative Boron-Free Core Integrated Within a Generic Small Modular Reactor. Doctoral Dissertation, Karlsruher Institut für Technologie (KIT), Karlsruhe, Germany, 2019.
9. U.S.NRC. *Appendix A to Part 50—General Design Criteria for Nuclear Power Plants*; U.S.NRC: Rockville, MD, USA, 2021.
10. Akbari-Jeyhouni, R.; Ochbelagh, D.R.; Gharib, A. Assessment of an integral small modular reactor during rod ejection accident by using DRAGON/PARCS codes. *Prog. Nucl. Energy* **2018**, *108*, 136–143. [CrossRef]
11. Campos-Muñoz, A.; Sanchez-Espinoza, V.H.; Redondo-Valerob, E.; Queral, C. Verification of the Coupled Code PARCS/TWOPORFLOW with Rod Ejection Accident Calculations for Small Modular Reactors. *Nucl. Sci. Eng.* **2024**, *199*, S777–S796. [CrossRef]
12. Alzaben, Y.; Sanchez-Espinoza, V.; Stieglitz, R. Analysis of a control rod ejection accident in a boron-free small modular reactor with coupled neutronics/thermal-hydraulics code. *Ann. Nucl. Energy* **2019**, *134*, 114–124.
13. Mercatali, L.; Huaccho, G.; Sanchez-Espinoza, V.-H. Multiphysics modeling of a reactivity insertion transient at different fidelity levels in support to the safety assessment of a SMART-like small modular reactor. *Front. Energy Res.* **2023**, *11*, 1130554. [CrossRef]
14. Ferrer, R.M. *CASMO5 Methodology Manual*; Studsvik Scandpower, Inc.: Idaho Falls, ID, USA, 2022.
15. Vanevenhoven, S.; Bahadir, T. *SIMULATE5 User's Manual Rev 16*; Studsvik Scandpower, Inc.: Idaho Falls, ID, USA, 2021.
16. Song, Y.; Sánchez-Espinoza, V.H. Safety-related Investigations Designing a Soluble-boron-free Small Modular Reactor Core at Equilibrium. *EPJ-Nucl. Sci. Technol.* **2026**, *12*, 6.
17. Bahadir, T. Development and Benchmarking of Transient Nodal Code SIMULATE5-K Neutron Kinetics Solver. In Proceedings of the PHYSOR, Pittsburgh, PA, USA, 15–20 May 2022.
18. OECD. State-of-the-art Report on Nuclear Fuel Behaviour Under Reactivity-initiated Accident Conditions. *NEA No.7575*; Nuclear Energy Agency: Boulogne-Billancourt, France, 2022.
19. Clifford, P.M. *Technical and Regulatory Basis for the Reactivity-Initiated Accident Acceptance Criteria and Guidance*; U.S. Nuclear Regulatory Commission (NRC): Rockville, MD, USA, 2015.
20. Bell, G.I.; Glasstone, S. *The Nuclear Reactor Theory*; Van Nostrand Reinhold Company: New York, NY, USA, 1970.
21. Diamond, D.; Bromley, B.; Aronson, A. *Studies of the Rod Ejection Accident in a PWR*; W-6382 1/22/02; Brookhaven National Laboratory: New York, NY, USA, 2002.
22. Song, Y. Safety-Related Investigations on a Soluble-Boron-Free Small Modular Reactor Core. Doctoral Dissertation, Karlsruhe Insititute of Technology (KIT), Karlsruhe, Germany, 2026.
23. Louis, H.K.; Refeat, R.M.; Hassan, M.I. Control rod shadowing effect in PWR core utilizing Urania-Gadolinia fuel. *Prog. Nucl. Energy* **2021**, *142*, 103993. [CrossRef]
24. Lamarsh, J.R. *Introduction to Nuclear Reactor Theory*; CiNii Research: Tokyo, Japan, 1966.
25. W.E. Company. *4. Reactor, AP1000 Design Control Document*; Rev. 18; W.E. Company: New York, NY, USA, 2011.
26. Muth, B. Parametric Study on Burnable Absorber Rod to Control Excess Reactivity for a Soluble Boron Free Small Modular Reactor. Doctoral Dissertation, Institute of Technology of Cambodia, Phnom Penh, Cambodia, 2016.
27. Song, Y.; Sánchez-Espinoza, V. Neutron-physical and safety-related core design optimization of a soluble-boron-free small modular reactor. In Proceedings of the 32nd International Conference on Nuclear Engineering—Volume 6, Weihai, China, 22–26 June 2025.
28. IAEA. *Design of the Reactor Core for Nuclear Power Plants*; Safety Standards Series No. SSG-52; IAEA: Vienna, Austria, 2019.
29. AREVA-NP. *AREVA Design Control Document Rev.5-Tier 2 Chapter 04-Reactor-Section 4.4 Thermal-Hydraulic Design*; UR NRC: Rockville, MD, USA, 2013.
30. KTA. Design of Reactor Cores of Pressurized Water and Boiling Water Reactors; Part 2: Neutron-Physical Requirements for the Design and Operation of the Reactor Core and Adjacent Systems. In *Safety Standards of the Nuclear Safety Standards Commission (KTA)*; Report No. 3101.2; KTA: Salzgitter, Germany, 2012.